ISSN 1330–0016
CODEN FIZBE7

PHENOMENOLOGICAL LOCAL POTENTIAL ANALYSIS OF π^+ SCATTERING

S. A. E. KHALLAF and A. A. EBRAHIM

Physics Department, Assiut University, Assiut 71516, Egypt

Received 9 October 2003; Accepted 12 September 2005
Online 16 February 2006

π^+-nucleus scattering cross section are calculated by solving a Schrödinger equation reduced from the Klein-Gordon equation. Local potentials are assumed, and phenomenological potential parameters are searched energy dependently for π^+ scattering from ^{12}C, ^{40}Ca, and ^{208}Pb to reproduce not only differential elastic cross sections but also inelastic and total and reaction cross sections at 800 MeV/c pion laboratory momentum. The collective model is used to calculate the angular distributions of differential inelastic cross sections for pions leading to the lowest 2^+ and 3^- states of ^{12}C. The deformation parameters and lengths are extracted and compared to the corresponding ones from other works. Local potentials well describe the scattering of pions from nuclei.

PACS numbers: 24.10.Ht, 25.40.Ny, 25.80.Dj UDC 539.126

Keywords: π^+-nucleus scattering, elastic, inelastic, differential cross sections, local potentials, collective model, scattering from ^{12}C, ^{40}Ca, and ^{208}Pb

1. Introduction

Pion-nucleus elastic scattering has been studied using a variety of theoretical methods to understand the pion-nucleus interaction and thereby the nuclear structure in the framework of the multiple scattering theory, by using elementary pion-nucleon scattering amplitude obtained from the pion-nucleon scattering data.

The optical potentials normally used in the Klein-Gordon equation for the pion-nucleus scattering are known to be nonlocal, particulary in the Δ-resonance region due to the p-wave nature of the resonance. However, it would be not only easier to visualize but also interesting if one could localize the nonlocal potential and look at the dynamics of the scattering from a different point of view.

Recently, Satchler [1] showed a method of reducing the Klein-Gordon equation to the form of a Schrödinger equation by redefining some kinematical quantities.

Elastic and inelastic scattering of positive and negative pions at several incident energies and for various target nuclei ranging from ^{40}Ca to ^{208}Pb were analyzed by using local potentials of the Woods-Saxon (WS) form [1]. It was concluded that the simple WS local potential model seems to be useful for pion-nucleus scattering without recourse to complexities of the nonlocal interactions.

On the other hand, in previous work [2, 3], the local potential of Johnson and Satchler [4] equivalent to the Kisslinger nonlocal potential [5] was used to successfully analyze the elastic scattering [2] of $\pi^{\pm}$ from ^{12}C, ^{16}O, ^{28}Si and ^{40,44,48}Ca in the pion kinetic energy range from 30 to 292 MeV. Elastic and inelastic scattering [3] of pions by ^{40,42,44,48}Ca and ^{54}Fe at 116, 180, and 292.5 MeV had also been analyzed. Good reproduction of the data was obtained for these nuclei without adjusting any free parameters of the optical potential. It was concluded that the use of a local optical potential equivalent to the Kisslinger one predicts well the cross sections of $\pi^{\pm}$ elastic and inelastic scattering with zero range DWUCK4 code [6].

In general, it is well known that a continuous array of phenomenological optical model potentials may account for the elastic data, making this simple model less than useful for pion reactions. As a further test of the uniqueness of the parameters obtained from the elastic scattering, angular distributions for the inelastic scattering data of pions using the collective model is done. When inelastic zero-range calculations are carried out, the ambiguity in parameters of the WS optical potential are greatly reduced.

The main purpose of the present work is to find optical-model sets of parameters of the phenomenological WS optical potential for π^+ scattering from ^{12}C, ^{40}Ca, and ^{208}Pb at about 800 MeV/c incident pion momentum. These parameters are required in distorted-wave analysis of inelastic reactions. Comparing this simple local potential with the local one exactly phase-shift equivalent to the Kisslinger potential, obtained by using the Krell-Ericson transformation method [7], which has been used for instance by Parija [8] and recently by Johnson and Satchler [4], one has another way to reduce the ambiguity in the parameters of the WS potential. Inelastic scattering of π^+ leading to the lowest 2^+ and 3^- states in ^{12}C are analysed using the collective model in terms of the conventional zero-range distorted-wave Born approximation (DWBA).

The method employed here is described in Subsect. 2.1, the results and discussion of the WS local potentials are given in subsections 2.2-2.4. We compare our phenomenological local potential with the local Kisslinger potential in Sect. 3 and the conclusions are presented in Sect. 4.

2. *Optical model analysis*

2.1. The model

In most works dealing with the solving of the Klein-Gordon equation, a so-called truncated Klein-Gordon equation is used, which means that terms quadratic in the

potentials are neglected compared to the energy of the pion. With this assumption, one gets [4]

$$\left\{-(\hbar\, c)^2\, \nabla^2 \,+\, 2\omega\, (V_N + V_C)\right\} \phi = (\hbar\, k\, c)^2\, \phi\,, \tag{1}$$

where ϕ is the distorted wave function for the relative motion between the pion and the target nucleus, V_C and V_N are the Coulomb and the nuclear potentials, respectively, and k is the relativistic center-of-mass momentum of the pion. ω is the total energy of the pion in the center-of-mass (c.m.) system, defined as [1]

$$\omega \,=\, \frac{M_\pi\, m_T}{M_\pi \,+\, m_T}\, c^2\,. \tag{2}$$

$m_{_T}$ is the target mass and the effective pion mass is $M_\pi \,=\, \gamma_\pi\, m_\pi$, where γ_π is [1]

$$\gamma_\pi = \frac{y \,+\, \gamma_\ell}{(1 + y^2 + 2\, y\, \gamma_\ell)^{1/2}}, \quad y \,=\, \frac{m_\pi}{m_T}, \quad \gamma_\ell \,= 1 + \frac{K_\ell}{m_\pi c^2}, \tag{3}$$

K_ℓ is the pion bombarding energy in the laboratory system and $\mathrm{m}_{_\pi}$ is the pion mass. Here $m_{_\pi}\, c^2$=139.6 MeV has been used. Satchler [1] introduced a reduced mass $\mu = \omega/\mathrm{c}^2$ and converted Eq. (1) to the form of Schrödinger equation

$$\left\{-\frac{\hbar^2}{2\mu}\nabla^2 \,+\, V_N \,+\, V_C\right\}\phi = E_{\mathrm{cm}}\, \phi, \tag{4}$$

for the scattering of two masses, M_π and m_T with center-of-mass kinetic energy $E_{\mathrm{cm}} \,=\, (\hbar\, k)^2/2\mu$. The incident pion bombarding energy was modified to $E_\ell \,=\, E_{\mathrm{cm}}(M_\pi + m_T)/m_T$, the so-called effective bombarding energy, so that a standard nonrelativistic optical model computer code could be used. Here, the DWUCK4 [6] and Hi-optim 94.2 [9] codes were used.

2.2. Results for phenomenological local potentials

The Woods-Saxon form of V_N in Eq. (4) can be written as

$$V_N(r) = -\frac{V}{1 + \exp(X_V)} \,-\, \mathrm{i}\, \frac{W}{1 + \exp(X_W)}\,, \tag{5}$$

with

$$X_j \,=\, (r \,-\, R_j)/a_j, \quad R_j = r_j\, A^{1/3} \quad (j \,=\, V,\, W)\,,$$

where r_j and a_j are the radius and the diffuseness parameters, respectively, and A is the target mass number. Here, V is the depth of the real part of the potential and W the corresponding depth for the imaginary part. Since pions are spinless particles, the spin-orbit term is not taken into account. V_C in Eq. (4) is the Coulomb potential due to a uniformly charged sphere of radius $R_C = 1.2\, A^{1/3}$ fm [3].

Optical model analyses were carried out here using the automatic search program Hi-optim 94.2 code due to Clarke [9]. This is a nonrelativistic program for local optical model calculations and needs as input, among other quantities, the mass and energy of the incident particle. In this work, we used for these two quantities the relativistically corrected values; the effective pion mass M_π and the effective bombarding energy E_ℓ, as described before.

There are six adjustable parameters in Eq. (5). We fixed them by using a χ^2-value defined by

$$\chi^2 = \frac{1}{N} \sum_{i=1}^{N} \left(\frac{\sigma^i_{\rm exp} - \sigma^i_{\rm th}}{\Delta\sigma^i_{\rm exp}} \right)^2 , \tag{6}$$

this χ^2-value is evaluated at each energy, and given in Table 1. The potential parameters are adjusted so as to minimize the χ^2. In Eq. (6), N is the total number of experimental points, $\sigma^i_{\rm exp}$'s ($\sigma^i_{\rm th}$'s) and $\Delta\sigma^i_{\rm exp}$ are the experimental (theoretical) cross sections and uncertainties, respectively. Normalization uncertainties for the data are not included in the fitting, but we provide overall scale uncertainty of 10 % [1, 10].

TABLE 1. Woods-Saxon optical-potential parameters for π^+ scattering on ^{12}C and ^{40}Ca at 800 MeV/c and on ^{208}Pb at 790 MeV/c. Five selected sets that minimize χ^2 are given for each pion lab momentum. Fits are shown in Fig. 1. A positive real potential is attractive and a positive imaginary potential is absorptive.

Set	V (MeV)	r_v (fm)	a_v (fm)	W (MeV)	r_w (fm)	a_w (fm)	χ^2
π^+ ^{12}C at 800 MeV/c							
1	13.106	1.40	0.5260	68.328	0.9096	0.4711	1.013
2	15.2656	1.20	0.3660	92.978	0.8118	0.4938	5.29
3	28.654	1.00	0.5214	111.188	0.7590	0.5250	3.92
4	32.211	0.952	0.5554	130.71	0.7174	0.5427	3.95
5	−6.475	1.10	0.3130	112.625	0.7673	0.5362	4.99
π^+ ^{40}Ca at 800 MeV/c							
1	11.054	1.2862	0.3123	48.246	1.033	0.5244	3.14
2	12.774	1.2790	0.4000	52.761	1.0292	0.5405	4.21
3	−36.00	1.00	0.500	42.819	1.1178	0.5333	2.24
4	−15.943	1.102	0.4621	43.198	1.0579	0.5855	3.99
5	−11.078	1.0779	0.4415	65.262	1.0063	0.6100	3.15
π^+ ^{208}Pb at 790 MeV/c							
1	−12.194	1.00	0.3020	298.783	0.8029	0.9035	3.15
2	−2.396	1.200	0.500	62.125	1.0828	0.7097	3.14
3	−3.521	1.00	0.5570	156.60	0.923	0.8488	2.97
4	−5.176	0.937	0.543	235.818	0.8458	0.8885	3.08
5	−6.90	0.815	0.5570	614.409	0.6677	0.9407	3.18

In searching for the parameters, we first kept the radius parameters r_i as 0.9 or 1.0 fm and the diffuseness a_i as 0.4 or 0.5 fm. When we could not get good fits to the data with these fixed parameters, we let them vary. We tried to find attractive (absorptive) potentials for the real (imaginary) part at all energies. It was possible to find attractive real potentials at 800 MeV/c for ^{12}C and ^{40}Ca, but repulsive real potentials were obtained at 790 MeV/c for ^{208}Pb. Satchler also obtained a repulsive Woods-Saxon potential for $\pi^{\pm}$ – ^{208}Pb scattering at 291 MeV. In both ^{12}C and ^{40}Ca at 800 MeV/c, the cross sections calculated with attractive real potentials are indistinguishable from the ones calculated with repulsive real potentials. In all cases under consideration, the imaginary part of the potential is found to be absorptive.

There is a well known ambiguity in determining the optical potential parameters [1, 11]. Due to the stronger absorption taking place in the nuclear surface region, different potentials can often fit the elastic scattering data equally well as long as they have similar values near the surface region. Such ambiguities are well known for other projectiles and have been noted for pions as well [1, 11].

Actually, we found that when we used only the differential elastic cross sections as the data to be fitted, the extracted potential parameters could not always reproduce the experimental reaction (σ_R) cross sections. However, when we included in the fitting σ_R as the data to be reproduced in addition to the differential cross section, the resulting potential parameters reproduced all cross sections quite well as shown in Fig. 1, with typical results for the parameters listed in Table 1.

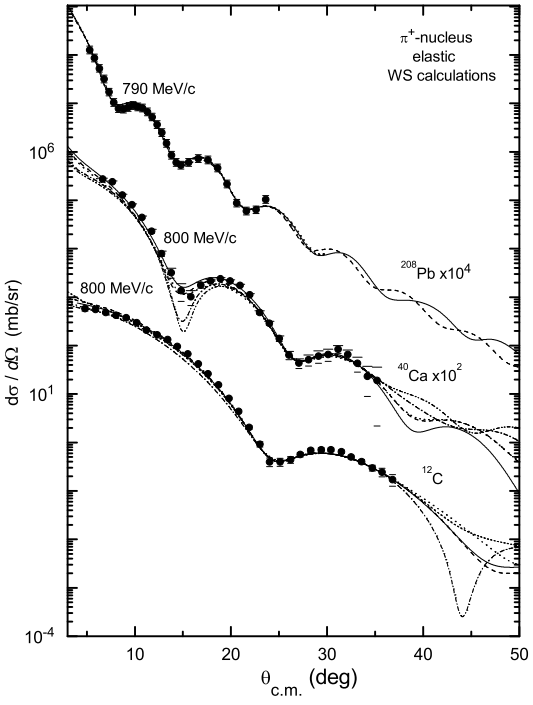

Fig. 1. Data for differential elastic cross section scattering at about 800 MeV/c π^+ *from* ^{12}C, ^{40}Ca *and* ^{208}Pb *Refs. [12, 13], compared with five curves computed with the WS local optical model parameter sets of Table 1. The solid curves show the predictions using set 1, dotted curves use set 2, dashed curves use set 3, dot-dashed curves use set 4, and dash-two dotted curves use set 5. In case of* ^{208}Pb *the dotted, dot-dashed, and dash-two dotted curves coincide with the solid one.*

For the inelastic π^+ scattering, the collective model of ^{12}C nucleus is considered here. The radial parts of the reaction potential are taken as the first derivative of the elastic potential given by Eq. (5), which produces good fits to the experimental elastic scattering data multiplied by a deformation parameter β_l, where l is the angular momentum transfer. β_l is decomposed into $\beta_{\rm real}$ and $\beta_{\rm imag}$ multiplied, respectively, by the real and imaginary parts of the reaction potential.

2.3. Elastic scattering calculations

In each case under consideration, many sets of parameters producing acceptable fits to experimental data are found with an attractive or a repulsive real potential and various values of χ^2. The imaginary potentials are always absorptive. This means that in any case the π^+ are absorbed by target nuclei at the considered energy. Only five of these sets for each target nucleus at certain incident momenta are given in Table 1. These given sets are selected according to the lowest minimum values of χ^2, prediction of the most reasonable fits to the inelastic scattering data and production of the nearest reaction cross sections σ_R to those found experimentally [12].

Figure 1 shows the angular distributions for π^+ elastic scattering differential cross sections from ^{12}C and ^{40}Ca at 800 MeV/c, and ^{208}Pb at 790 MeV/c calculated by Hi-optim 94.2 code [9], using the five sets of potential given in Table 1 compared to the experimental data [12, 13]. In Fig. 1, the solid curves show the predictions using set 1, dotted curves use set 2, dashed curves use set 3, dot-dashed curves use set 4, and dash-two dotted curves use set 5. The solid circles represent the experimental data [12, 13]. This figure shows for all cases considered here reasonable agreements between measured differential cross sections and those calculated with optical potential parameters given in Table 1.

Table 2 shows the predictions of the computer Hi-optim 94.2 code used in the present work for the partial-wave angular momentum $L_{1/2}$ corresponding to the strong absorption radius D. Predictions of that program for the real J_R and imaginary J_I volume integrals per nucleon of the target nucleus, the real Re $V_N(D)$ and Im $V_N(D)$ nuclear parts of potential at the distance D and the root-mean-square radii of the real $< r^2 >_R^{1/2}$ and imaginary $< r^2 >_I^{1/2}$ parts of the nuclear potential are also shown in Table 2. The strong absorption radius D is defined as [1]

$$\acute{k}\, D \,=\, [L_{1/2}\,(L_{1/2}\,+\,1)\,+\,\eta^2]^{1/2}\,+\,\eta, \quad \eta = Z_\pi Z_T\, e^2 \mu/\hbar^2\, \acute{k}, \tag{7}$$

where $\acute{k}$ is the wave number, η is the the Sommerfeld parameter and $L_{1/2}$ is the angular momentum for which Re(S_ℓ) is equal to $\frac{1}{2}$ (S being the matrix describing the scattering). The values of D calculated by the relation (7) from the optical parameters obtained in this work are presented in Table 2. In most cases, these values are the same to better than 1 % for a given nucleus, whatever family or form of the imaginary potential is used. It is well known that at the strong absorption radius D the incident particle has a 50 % probability of being absorbed by the target nucleus.

TABLE 2. Derived quantities for π^+ scattering from ^{12}C, ^{40}Ca, and ^{208}Pb using parameter sets in Table 1. For definitions of these quantities, see the text.

Set	$L_{1/2}$	D (fm)	J_R (MeV fm^3)	J_I	Re $V_N(D)$ (MeV)	Im $V_N(D)$ (MeV)	$< r^2 >_R^{1/2}$ (fm)	$< r^2 >_I^{1/2}$ (fm)
π^+ ^{12}C at 800 MeV/c								
1	9.097	2.397	155.3	264.2	12.92	51.62	3.16	2.38
2	9.134	2.406	105.8	288.4	15.22	56.52	2.53	2.33
3	9.382	2.468	147.9	316.2	23.12	55.43	2.63	2.37
4	9.572	2.515	155.8	343.8	23.72	75.22	2.67	2.39
5	9.409	2.475	33.89	334.3	−6.25	54.92	2.63	2.37
π^+ ^{40}Ca at 800 MeV/c								
1	14.9	3.927	88.09	230.9	11.02	36.84	3.60	3.36
2	15.25	4.014	103.2	252.9	12.53	36.71	3.70	3.39
3	15.45	4.065	155.6	254.38	−22.72	34.81	3.24	3.56
4	15.00	3.951	83.49	234.9	−13.86	32.82	3.37	3.54
5	15.79	4.15	56.45	311.3	−8.645	38.52	3.29	3.50
π^+ ^{208}Pb at 790 MeV/c								
1	30.1	7.84	44.83	751.76	−0.9189	20.90	4.72	4.99
2	28.83	7.529	15.56	316.79	−1.910	29.70	5.81	5.63
3	29.78	7.767	13.72	546.29	−0.601	24.80	5.03	5.28
4	29.98	7.818	16.24	669.995	−0.388	22.80	4.71	5.10
5	30.24	7.883	15.145	1022.12	−0.109	17.60	4.28	4.65

The following features are noted:

1. From Tables 1 and 2, it is seen that both the depth of the real part of the optical potential V_N and the corresponding volume integral per nucleon of the target nucleus J_R decrease with the increase of the mass number of the target nucleus. This behaviour was also noticed for ^{3}He-nucleus scattering [14]. This potential is repulsive for ^{208}Pb and for many cases for ^{40}Ca. The imaginary potential is stronger and absorptive in all cases.

2. From Table 2, it is clear that for each case under consideration $L_{1/2}$ and D are approximately constant when using any of the five sets. D and $L_{1/2}$ increase as the mass number of the target nucleus increases. The increase of D values as mass number of the target nucleus increases is consistent with that for elastically scattered ^{3}He from a variety of nuclei at 25 MeV [14].

3. The optical model calculation also gives reaction cross sections σ_R, as listed in Table 3. The WS local optical model gives values of σ_R very close to those estimated by Kisslinger local potential [4]. This indicates that the imaginary part of the optical model used here, which is strongly correlated to σ_R, is well predicted. Investigating the elastic scattering of negative pions from ^{12}C at thirteen energies ranging from 120 to 766 MeV, Hong and Kim [15] found that the following relation is roughly valid

$$\sigma_T \;=\; 1.59\,\pi\,D^2,$$

TABLE 3. Total and reaction cross sections (in mb*) calculated using both WS and Kisslinger local potentials for* ^{12}C, ^{40}Ca, *and* ^{208}Pb *at about 800* MeV/*c.*

		WS cals.		Kisslinger cals.	
Nucleus	Set	σ_R	σ_T	σ_R	σ_T
^{12}C	1	201.2	304.12	232.7	321.18
	2	205.9	302.51		
	3	219.3	308.64		
	4	229.6	352.87		
	5	224.5	314.68		
^{40}Ca	1	589.5	881.96	613.7	901.32
	2	571.6	880.12		
	3	600.0	874.56		
	4	605.9	872.74		
	5	609.8	891.49		
^{208}Pb	1	1809.3	3149.5	1850.4	3175.4
	2	1799.6	3136.3		
	3	1839.8	3129.6		
	4	1817.2	3122.9		
	5	1820.8	3154.6		

with $D = r_s A^{1/3}$. Here, in case of π^+ scattering from ^{12}C, ^{40}Ca, and ^{208}Pb at about 800 MeV/c and using the mean values of D and σ_T shown in Tables 2 and 3, it is found that 1.69 is more suitable than 1.59 and r_s=1.071, 1.176, and 1.311 fm for ^{12}C, ^{40}Ca and ^{208}Pb, respectively.

4. In the case of ^{12}C target, the lightest nucleus considered here, $< r^2 >_R^{1/2}$ shown in Table 2 is longer than the corresponding strong absorption radius D and both of them are greater than $< r^2 >_I^{1/2}$. Also for each set of optical potential parameters, $< r^2 >_R^{1/2}$ is longer than the corresponding value for nuclear matter $< r^2 >_m^{1/2}$ given in Ref. [16], while $< r^2 >_I^{1/2}$ shown in Table 2 are approximately equal to $< r^2 >_m^{1/2}$ of Ref. [16]. The present predictions of $< r^2 >_R^{1/2}$ and $< r^2 >_I^{1/2}$ shown in Table 2 for ^{40}Ca and ^{208}Pb are shorter than $< r^2 >_m^{1/2}$ of Ref. [16]. This may suggest that pions start interaction with the lightest nuclei outside the nuclear matter.

5. The imaginary potentials obtained for these data sets are very ambiguous. The π^+ cross sections could not be reproduced by use a nonabsorptive imaginary potential (W <0) or a purely real one (W=0). However, the scattering by these potentials is quite strongly influenced by the imaginary potential. It was found in the cases studied here that quite good fits to the scattering data could be obtained with a purely imaginary potential (V=0), as shown by the dashed curves in Fig. 2. In each case, the Coulomb potential V_C is included. As it is expected, the Coulomb

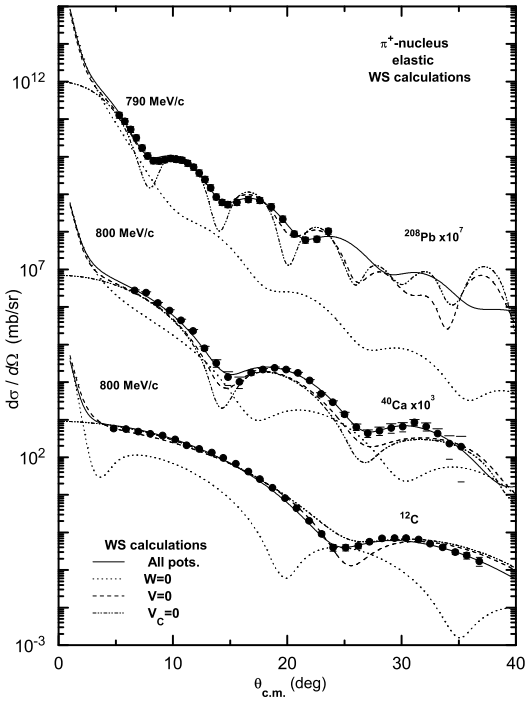

Fig. 2. As in Fig. 1 but using only set 1 parameters. The solid curves represent the differential elastic scattering cross sections using the whole potentials; nuclear and Coulomb potentials. The dotted curves use the real nuclear (W=0) and Coulomb potentials. The dashed curves use the imaginary nuclear (V=0) and Coulomb potentials. The dot-dashed curves use the nuclear potentials only (V_C=0).

potential effect on the predicted differential cross sections increases as the atomic number of the target nucleus increases. The ripples in the differential cross sections due to V_C=0 in the case of ^{208}Pb, as shown as dot-dashed curves, are much stronger compared to those in the case of ^{40}Ca, while in the case of ^{12}C these ripples are quite damped. It can be concluded that the differential cross sections predicted with the imaginary part of the optical potential plus the Coulomb potential as shown as dashed curves (V=0) are dominant with respect to the corresponding ones with $W = 0$, as shown by the dot curves in Fig. 2.

6. Re $V_N(D)$ and Im $V_N(D)$ given in Table 2 for all considered cases show that the drop of the real part of the potential with respect to V for a certain set is much less than that of the imaginary part with respect to W at the same distance D, especially for ^{12}C and ^{40}Ca. This behaviour is also reflected by Fig 3.

Also shown in Fig. 3 are the resulting $\pi^+ - ^{12}$C WS local potentials at 800 MeV/c pion lab momentum using the five sets. Set 1 of WS optical potential parameters yield real and imaginary potential around the strong absorption radius D approximately the same as those predicted by the local Kisslinger potential. They have one feature in common, the tails of the potentials are almost identical. The agreement in the interior region is poor. This indicates that this region does not participate in the scattering mechanism. This result is similar to that of nucleon-nucleus scattering, see e.g. Ref. [17], nucleus-nucleus [18], and pion scattering [1]. From that figure it is seen that in this case the imaginary part is quite shallow and everywhere absorptive, while the real part is attractive with sets 1 – 4 and repulsive only with

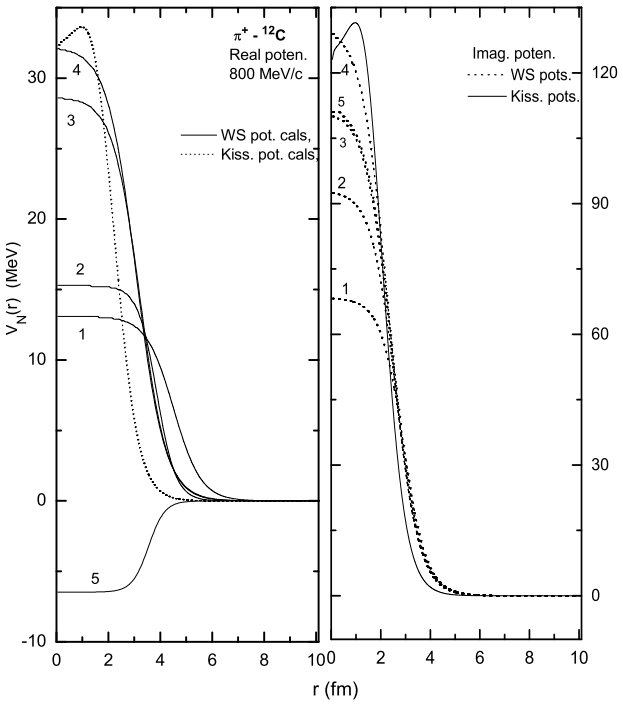

Fig. 3. WS local optical potentials computed at 800 MeV/*c* π^+ *scattered from* ^{12}C *with the parameter sets of Table 1, compared to the Kisslinger local potential. Left for the real potential, the full curves are for the WS and the dotted curve for the Kisslinger local one. Right for the imaginary potential, the dotted curves are for the WS and the solid curve for the Kisslinger local potential.*

set 5. The imaginary part is deeper and rapidly decreasing, while the real part is shallower and wider. The imaginary parts of these five potentials are approximately identical in the surface region of ^{12}C. This is reflected by the parameters given in Table 1. The radial shape of the real and the imaginary parts both follow the density ρ(r). Previously, it was found that both real and imaginary potentials are repulsive for $K^+ - {}^{12}C$ at 300 MeV [Fig. 3.3 of Ref. [19]], while the real potential was repulsive and the imaginary one was attractive for $K^+ - {}^{208}Pb$ at 200 and 500 MeV [20].

2.4. Inelastic scattering calculations

Since there are no available data for inelastic scattering from ^{40}Ca and ^{208}Pb at around 800 MeV/*c* at the present time, we considered here the case of ^{12}C. The potential parameter sets listed in Table 1 are used to calculate the inelastic scattering by the first derivative of the elastic potential given by Eq. (5) multiplied by a deformation parameter β_l where l(=2 or 3) is the multipolarity.

Collective-model calculations are carried out for inelastic scattering to the lowest 2^+ and 3^- states of ^{12}C. DWBA calculations are made for π^+ at 800 MeV/*c* using all potential sets of ^{12}C in Table 1. These sets, in spite of a wide variation in the parameter values, are found to give comparable and acceptable fits to the corresponding elastic scattering data. Shown in Fig. 4 are DWBA calculations using the DWUCK4 program [6] fits to the inelastic angular distribution with the

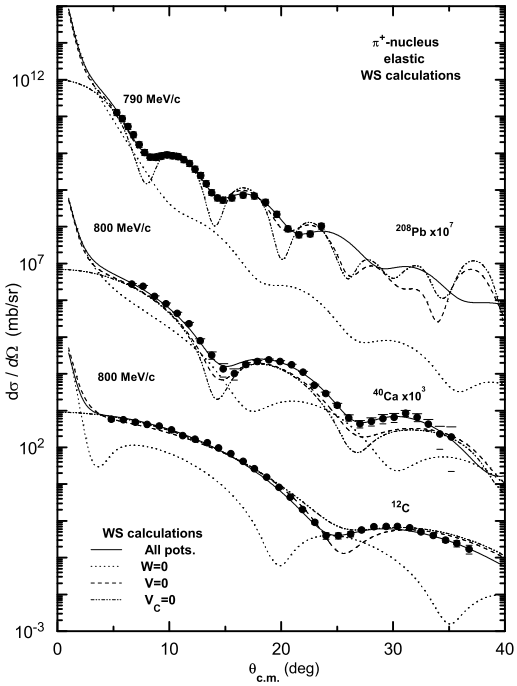

Fig. 4. As in Fig. 1 but for differential inelastic cross sections at 800 MeV/*c* π^+ *Ref. [13] exciting the 4.44* MeV 2^+ *and 9.64* MeV 3^- *states of* ^{12}C.

excitation of the (2^+; 4.44 MeV) and (3^-; 9.64 MeV) states in ^{12}C. These calculations result for (2^+; 4.44 MeV) in acceptable fits at scattering angles beyond $\theta_{\rm cm} \approx 20^\circ$ and (3^-; 9.64 MeV) states beyond $\theta_{\rm cm} \approx 30^\circ$, respectively, as shown in Fig. 4. Only set 1 yields approximately good fit with data over the wide available

TABLE 4. Deformation lengths (in fm*) for the 4.44* MeV 2^+ *and 9.64* MeV 3^- *states of* ^{12}C *at 800* MeV/*c compared to those predicted by others.*

State	Set	Present				Others	
		WS cals.		Kissl. cals.			
		$\delta_{\rm real}$	$\delta_{\rm imag.}$	$\delta_{\rm real}$	$\delta_{\rm imag.}$	δ	Ref.
2^+	1	1.969	1.0829	1.732	1.113	1.0-1.63	[23]
	2	1.676	0.9665			0.978-1.725	[24]
	3	1.397	0.9036			1.12-1.97	[25]
	4	1.329	0.8541				
	5	1.536	0.9135				
3^-	1	1.731	0.9788	1.449	1.102	0.955-1.512	[24]
	2	1.484	0.8735			0.65-1.23	[25]
	3	1.236	0.8167				
	4	1.177	0.7719				
	5	1.359	0.8256				

scattering angles with deformation parameters that agree with other studies of ^{12}C nucleus. Deformation parameters obtained from the present work are $\beta_{\rm real}$=0.61 and $\beta_{\rm imag}$=0.52 for the 2^+ state, while $\beta_{\rm real}$=0.54 and $\beta_{\rm imag}$=0.47 for the 3^- state. Other works [21, 22] gave β_2=0.40 to 0.59±0.05 for the 2^+ state and β_3=0.37 to 0.48 for the 3^- state.

To calculate deformation lengths from parameters of Table 1 for both 2^+ and 3^- states, we used the relations

$$\delta_{\rm real} = \beta_{\rm real} r_v A^{\frac{1}{3}},$$
$$\delta_{\rm imag.} = \beta_{\rm imag.} r_w A^{\frac{1}{3}}, \tag{8}$$

where r_v and r_w are given in Table 1. The resulting deformation lengths are listed in Table 4 with those estimated by the Kisslinger local potential calculations, and these values are very similar to those of Refs. [23 – 25].

3. *Comparison with local potentials equivalent to the Kisslinger potential*

For the nuclear potential V_N in Eq. (1), the Kisslinger form [5] of the potential has been frequently used, which can be written as

$$V_N = \frac{(\hbar c)^2}{2\omega}\left\{q(r) + \nabla\cdot\alpha(r)\nabla\right\}. \tag{9}$$

The quantity q(r) mainly results from the s-wave part and α(r) results from the p-wave part of the pion-nucleon interaction, $q(r)$ and α(r) can be expressed in terms of the target-nuclei density distributions and their gradients. Both are complex and energy dependent and are given in detail in Ref. [4]. Previously, Hong and Kim [15] used s- and p-waves only to analyze elastic scattering of negative pions from ^{12}C in the energy range of 120 to 766 MeV.

By rewriting the pion distorted wave function $\phi(r)$ in Eq. (1) as

$$\phi(r) \;=\; P(r)\,\psi(r), \tag{10}$$

with the Perey factor $P(r) = [1 - \alpha(r)]^{-1/2}$, one can get a Schrödinger equation for $\psi(r)$,

$$\left\{-\frac{\hbar^2}{2\mu}\nabla^2 + U_L + V_C\right\}\psi = E_{\rm cm}\,\psi\,, \tag{11}$$

where μ and $E_{\rm cm}$ are the same as in Eq. (4). Here, U_L is a local potential depending only on r as follows

$$U_L(r) = \frac{(\hbar c)^2}{2\omega}\left\{\frac{q(r)}{1-\alpha(r)} - \frac{k^2\,\alpha(r)}{1-\alpha(r)} - \frac{\frac{1}{2}\,\nabla^2\,\alpha(r)}{1-\alpha(r)} - \left(\frac{\frac{1}{2}\nabla\,\alpha(r)}{1-\alpha(r)}\right)^2\right\} + \frac{\alpha(r)\,V_C}{1-\alpha(r)}\,. \tag{12}$$

The second term in the last equation is the Coulomb correction. The pion-nucleon scattering amplitude depends on complex first- and second-order interaction parameters. The first-order interaction parameters are related to the free pion-nucleon scattering parameters through the phase shifts in the form described in Ref. [26] and the phase shifts are calculated according to Eq. (5) in Ref. [27]. The first-order interaction parameters are then used to generate the complex local potential U_L in Eq. (12), using the expressions from Ref. [4]. In this work, the second-order interaction parameters are neglected [28], while these parameters are required only at lower energies $T_\pi \leq 80$ MeV and they make no differences in the calculations at higher energies, so they are here set to be zero [2, 29]. We took the three-parameter Fermi shape 3PF density distributions of the considered nuclei from Refs. [2, 30].

The real and imaginary parts of U_L calculated with Kisslinger local potential are shown in Fig. 3 as dotted-and-solid curves for the real and imaginary potentials, respectively, together with those calculated using the WS parameters.

Figure 5 displays the predictions of the differential elastic cross sections of π^+ from ^{12}C, ^{40}Ca, and ^{208}Pb using both set 1 of WS of Table 1 and the local Kisslinger

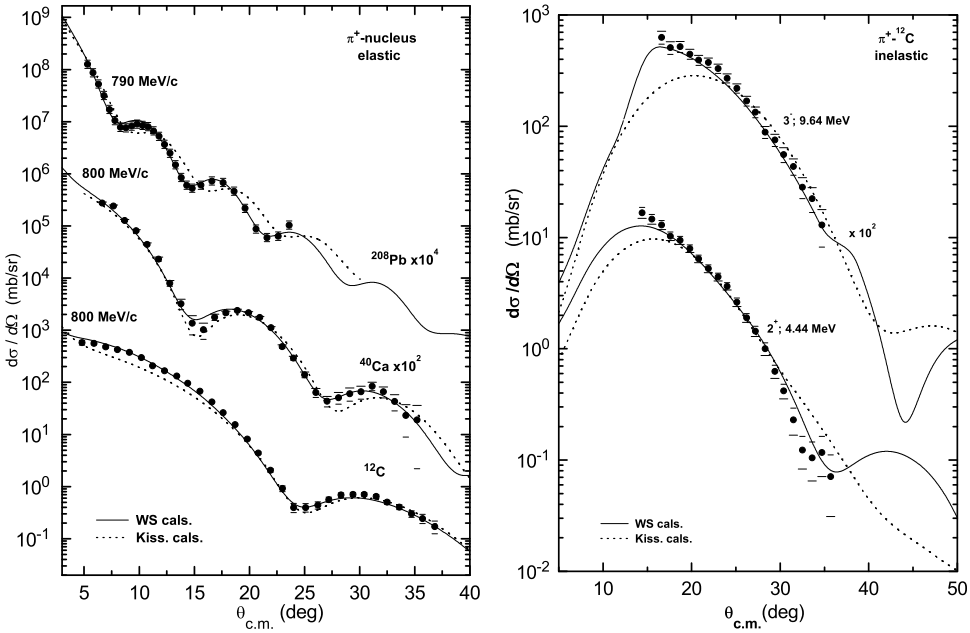

Fig. 5 (left). Differential elastic cross sections at about 800 MeV/*c* π^+ ^{12}C, ^{40}Ca, *and* ^{208}Pb *Refs. [12, 13], compared to calculations using set 1 parameters of WS local potential as solid curves and those computed using the Kisslinger local potential as dashed curves.*

Fig. 6. As in Fig. 5, but for differential inelastic of π^+ *exciting the 4.44* MeV 2^+ *and 9.64* MeV 3^- *states of* ^{12}C.

potentials. The two forms for the optical potential models give reasonable agreement with the data of Refs. [12, 13], but the local WS potential predictions as the solid curves, using set 1 parameters, seem to be better for all nuclei considered in the present work. It was concluded in Ref. [27] that the disagreement between the data and the local Kisslinger potential calculations at high energies refer to the parameters used to calculate the pion-nucleon phase shifts. These parameters are not adequate for higher pion energies and that may seriously affect the results of calculations.

Also shown in Fig. 6 are the inelastic scattering data for the 2^+ and 3^- states in ^{12}C at 4.44 and 9.64 MeV, respectively, compared with both types of optical potentials. Those were calculated using the πN phase shifts and local Kisslinger potential, shown as dotted curves, and the set 1 of phenomenological potentials of Table 1 as solid curves. They yield reasonable agreement with the data, but the WS calculations are still in a better agreement as they do for elastic scattering.

The DWUCK4 code [6] using the present first-order local optical potential calculates the reaction cross sections σ_R for positive pions on ^{12}C, ^{40}Ca, and ^{208}Pb at about 800 MeV/c. Following the same procedure, the total cross section σ_T is calculated according to the well known relation [24]

$$\sigma_T = \frac{2\pi}{\acute{k}^2} \sum_L (2L + 1) \left[1 - \mathrm{Re}\, S_L\right], \tag{13}$$

where S_L is the projectile-nucleus non-Coulomb amplitude. The results of the total and reaction cross section calculated with both types of local potentials are shown in Table 3. Comparing the present results for the total cross section σ_T in the case of ^{40}Ca shown in Table 3 to our previous results given in Table IV of Ref. [3] for the same quantity but at lower energies, it is clear that σ_T for pion scattering at 800 MeV/c is smaller than σ_T at 116, 180, and 292.5 MeV. This means that the mean free path λ of pions in the resonance region is shorter than λ at higher energies.

The resulting deformation lengths from the Kisslinger potentials determined by visually adjusting the calculations to reproduce the data are listed in Tables 4 compared to those obtained from WS calculations using parameter sets given in Table 1. Deformation lengths determined here using both types of potentials are very similar to those obtained from Refs. [23 – 25].

4. *Conclusion*

We assumed the Woods-Saxon form of phenomenological local potentials in solving a Schrödinger equation reduced from the Klein-Gordon equation and searched for the potential parameters of π^+ scattering on nuclei. The calculated cross sections reproduced the experimental data quite well for the considered nuclei. The imaginary parts of the five sets are identical in the outer nuclear surface region. Table 1 shows that at higher energies the real part of the phenomenological local potential becomes much smaller than the imaginary part.

Angular distributions of π^+ elastically scattered from ^{12}C, ^{40}Ca, and ^{208}Pb at about 800 MeV/c pion lab momentum are well reproduced by a six-parameter optical model using the Woods-Saxon shape for both the real and imaginary parts of the potential. The strong absorption radius and σ_R are found to be quite stable over a wide range of parameters. Elastic scattering calculations based on the Kisslinger local potentials are in a good agreement with data and found to be nearly indistinguishable from those of WS potentials, as shown in Fig. 5.

Angular distributions for pion inelastic scattering from ^{12}C have been studied at 800 MeV/c. The data are analysed using a collective model and the DWBA with two types of local potentials, one being a phenomenological whose parameters are determined by fitting the elastic scattering angular distributions, and the other using strengths determined from free πN phase-shift Kisslinger potential. The deformation lengths and parameters determined from the present analysis are in agreement with deformations determined using other probes. This collective model analysis is successful in its description of the reaction dynamics and the structure of the collective, $N = Z$ nucleus.

We again stress that the phenomenological local potentials obtained here are not necessarily unique, but this simple local potential model seems to be a useful one for π^+ – nucleus scattering without recourse to the complexities of the non-local interaction. These parameters allow others to use local zero-range optical potentials for a range of reactions involving pions.

In general, it can be concluded from this work and from other works [1 – 3,11,15] that local potentials describe well the scattering of pions from nuclei.

References

[1] G. R. Satchler, Nucl. Phys. A **540** (1992) 533.

[2] S. A .E. Khallaf and A. A. Ebrahim, Phys. Rev. C **62** (2000) 024603.

[3] S. A. E. Khallaf and A. A. Ebrahim, Phys. Rev. C **65** (2002) 064605.

[4] M. B. Johnson and G. R. Satchler, Ann. Phys. N. Y. **248** (1996) 134.

[5] L. S. Kisslinger, Phys. Rev. **98** (1955) 761.

[6] P. D. Kunz, DWBA code DWUCK4 University of Colorado (unpublished).

[7] M. Krell and T. E. O. Ericson, Nucl. Phys. B **11** (1969) 521.

[8] B. C. Parija, Phys. Rev. C **28** (1983) 453.

[9] N. M. Clarke, Hi-optim 94.2 code (1994) University of Birmingham, England (unpublished).

[10] K. G. Boyer et al., Phys. Rev. C **24** (1981) 598; K. G. Boyer et al., Phys. Rev. C **29** (1984) 182; C. L. Morris et al., Phys. Rev. C **24** (1981) 231.

[11] Md. A. E. Akhter, Sadia Afroze Sultana, H. M. Sen Gupta and R. J. Peterson, J. Phys. G **27** (2001) 755.

[12] T. Takahashi et al., Phys. Rev. C **51** (1995) 2542.

[13] D. Marlow et al., Phys. Rev. C **30** (1984) 1662.

[14] J. Vernotte, G. Berrier-Ronsin and J. Kalifa, Nucl. Phys. A **390** (1982) 285.

[15] S. W. Hong and B. T. Kim, J. Phys. G **25** (1999) 1065.

[16] G. R. Satchler and W. G. Love, Phys. Rep. **55** (1979) 183.

[17] I. Brissaud, L. Bimbot, Y. Le Bornec, B. Tatischeff and N. Willis, Phys. Rev. C **11** (1975) 1537.

[18] Bikash Sinha, Phys. Rev. C **11** (1975) 1546.

[19] C. B. Dover and G. E. Walker, Phys. Reports **89** 1 (1982) 1.

[20] C. B. Dover and P. J. Moffa, Phys. Rev. C **16** (1977) 1087.

[21] R. E. Chrien, R. Sawafta, R. J. Peterson, R. A. Michael and E. V. Hungerford, Nucl. Phys. A **625** (1997) 251.

[22] R. J. Sobie et al., Phys. Rev. C **30** (1984) 1612.

[23] S. A. E. Khallaf, A. M. A. Nossair, A. A. Ebrahim and Awad A. Ebraheem, Nucl. Phys. A **714** (2003) 412.

[24] A. A. Ebrahim and S. A. E. Khallaf, Phys. Rev. C **66** (2002) 044614.

[25] S. M. Smith, G. Tibell, A. A. Cowley, D. A. Goldberg, H. G. Pugh, W. Reichart and N. S. Wall, Nucl. Phys. A **207** (1973) 273, and references therein.

[26] J. Bartel, M. B. Johnson and M. K. Singham, Ann. Phys. N.Y. **196** (1989) 89; S. J. Greene et al., Phys. Rev. C **30** (1984) 2003; R. A. Gilman, Ph.D. dissertation, University of Pennsylvania (1985).

[27] A. A. Ebrahim and S. A. E. Khallaf, Acta Phys. B **31** (2000) 2187.

[28] O. Meirav, E. Friedman, R. R. Johnson, R. Olszewski and P. Weber, Phys. Rev. C **40** (1989) 843.

[29] A. A. Ebrahim and R. J. Peterson, Phys. Rev. C **54** (1996) 2499.

[30] B. M. Preedom et al., Phys. Rev. C **23** (1981) 1134.

[31] F. Hinterberger, G. Mairle , U. Schmidt-Rohr, G. J. Wagner and P. Turek, Nucl. Phys. A **115** (1968) 570.

FENOMENOLOŠKA ANALIZA S LOKALNIM POTENCIJALOM RASPRŠENJA π^+

Izračunali smo udarne presjeke za raspršenje π^+-jezgra kao rješenja Schrödingerove jednadžbe koju smo izveli iz Klein-Gordononove jednadžbe. Primijenili smo lokalne potencijale, a parametre fenomenološkog potencijala smo odredili u ovisnosti o energiji za raspršenje π^+ na ^{12}C, ^{40}Ca i ^{208}Pb, tražeći sklad ne samo s elastičnim diferencijalnim udarnim presjecima, već i s totalnim i reakcijskim udarnim presjecima za pione s laboratorijskim impulsom 800 MeV/c. Primijenili smo kolektivni model za računanje kutne ovisnosti neelastičnih diferencijalnih udarnih presjeka za najniža 2^+ i 3^- stanja ^{12}C. Izveli smo parametre i duljine deformacije koje uspored ¯ujemo s odgovarajućim vrijednostima drugih radova. Lokalni potencijali dobro opisuju raspršenje piona u jezgrama.